Microwave Engineering
Ulm University

ulm university universität
uulm

Radar Imaging Using Electrically Large Arrays With High Range Resolution at 160 GHz

André Dürr, Benedikt Schneele, Dominik Schwarz, and Christian Waldschmidt

DOI: 10.1109/EuRAD48048.2021.00090

Radar Imaging Using Electrically Large Arrays With High Range Resolution at 160 GHz

André Dürr[1], Benedikt Schneele, Dominik Schwarz, and Christian Waldschmidt
Institute of Microwave Engineering, Ulm University, 89081 Ulm, Germany
[1]andre.duerr@uni-ulm.de

***Abstract* — In order to improve the resolution of imaging radars, electrically large arrays and high absolute bandwidths are required. At a large off-boresight angle of the incident wave, the difference in path length at the antennas becomes a multiple of the range resolution of the radar. Consequently, the radar responses of the targets at the different receiving channels are distributed over a large number of range bins, depending on the direction-of-arrival (DoA) of the target echo. Applying conventional signal processing, the resolution of the radar is considerably reduced. In this paper, the key aspects of DOA estimation are discussed when radars with both a large aperture size and a high absolute bandwidth are employed. A signal processing method is proposed avoiding errors that occur in conventional DOA estimation techniques. As shown by measurements, an angular resolution of 0.4° can be achieved with an array size of $200\,\lambda_0$ and a bandwidth of 10 GHz.**

***Keywords* — Direction-of-arrival (DoA) estimation, imaging radar, large antenna arrays, millimeter wave radar, multiple-input multiple-output (MIMO) radar.**

I. Introduction

Future radar applications require radar sensors that provide a high resolution in range, velocity, and angle. To realize high absolute bandwidths and electrically large apertures at compact physical dimensions, operating frequencies above 100 GHz are used [1], [2], [3]. In most applications, the DoA estimation is performed via digital beamforming at the receiver side. In order to separate close targets in the same range-velocity bin, the angular resolution has to be enhanced.

For typical MIMO radars, the difference in path length of the incident wave at the antenna elements is smaller than the range resolution of the radar [4], [5], [6]. However, employing high-resolution radars at operating frequencies above 100 GHz with large apertures, the difference in path length between adjacent antenna elements exceeds the range resolution of the radar, in particular for off-boresight angles of the received target echo [3], [7]. Due to these boundary conditions, the radar responses at the different virtual channels are distributed over a large number of range bins reducing the imaging performance of the radar. Range cell migration is also known from synthetic aperture radar, where images are often reconstructed by means of the back-projection algorithm [8].

In this paper, the performance degradation and problems related to high-resolution imaging radars with large apertures and high bandwidths are discussed when conventional narrowband beamforming is applied. An error correction method is proposed that allows to recover the full theoretical resolution. The effectiveness of the proposed error correction method is finally demonstrated by measuring an extended target, which represents multiple target reflections.

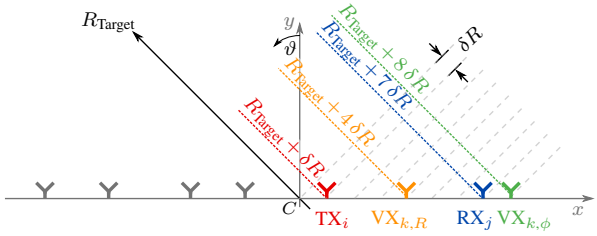

Fig. 1. K-th virtual antenna position ($\text{VX}_{k,\phi}$ and $\text{VX}_{k,R}$) with respect to the occurring difference in phase ϕ and with respect to the measured mean distance R resulting from one exemplary TX_i-RX_j combination and a target at distance R and angle ϑ from the array center C. The array is significantly larger than the range resolution δR of the radar.

II. Range-Angle Coupling Effect

In Fig. 1, the coordinate system with an exemplary transmitter (TX_i) and receiver (RX_j) and the resulting virtual antennas ($\text{VX}_{k,\phi}$ and $\text{VX}_{k,R}$) is shown for a target in the far-field at a distance R and angle ϑ from the array center C. The DoA of a target is given by a phase relation between the received signals at the RX antennas. In case of MIMO radars, the phase ϕ of the received signal at an exemplary virtual receive antenna $\text{VX}_{k,\phi}$ at the position $x_{\text{VX}_{k,\phi}}$ is composed of the sum of the signal phases at the corresponding TX and RX antennas. The k-th virtual antenna position $x_{\text{VX}_{k,\phi}}$ is given by a spatial convolution of the locations of the corresponding TX and RX antenna locations x_{TX_i} and x_{RX_j} [9].

However, due to the two-way propagation, the measured distance is only half of the path length of the signal from the TX antenna to the target and back to the RX antenna. This allows the definition of a distance-related virtual antenna position $x_{\text{VX}_{k,R}}$, which is located at half of the distance to the array center compared to the phase-related virtual antenna position $x_{\text{VX}_{k,\phi}}$. The additional path difference ΔR_k of the signal at the k-th VX antenna $x_{\text{VX}_{k,R}}$ is given by

$$\Delta R_k = x_{\text{VX}_{k,R}} \cdot \sin(\vartheta) = \frac{x_{\text{VX}_{k,\phi}}}{2} \cdot \sin(\vartheta) \qquad (1)$$

for a plane wave impinging on the array under the angle ϑ with respect to the array center C. Considering a system as shown in Fig. 1 having a range resolution δR smaller than the additional path difference at the distance-related virtual antenna $\text{VX}_{k,R}$, the targets are distributed over several range bins depending

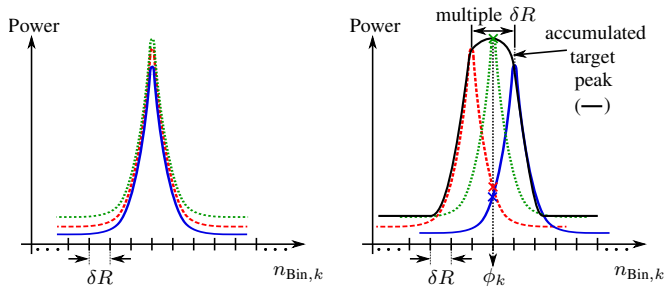

Fig. 2. Radar response for three exemplary virtual channels (——,- - -,·····): (a) Target in boresight direction ($\vartheta = 0°$) and (b) target in off-boresight direction ($|\vartheta| \gg 0°$ and therefore $\Delta R_k \gg \delta R$).

on the incidence angle ϑ (see Fig. 2). The measured range is coupled to the incidence angle of the target echo. This is denoted as range-angle coupling effect.

In common radar processing the range-Doppler matrices of each virtual channel are non-coherently accumulated into a single range-Doppler matrix [9]. The accumulated matrix contains information from all channels and provides a basis to extract possible targets. Afterwards, the phase values of all virtual channels are extracted from this single range bin where the target was determined and are fed into a DoA estimator. In the given case this procedure leads to a significant degradation of the resolution for targets located at off-boresight angles. As can also be seen in Fig. 2 (b), the phase values ϕ_k of certain virtual channels (here: —— and - - -) are taken from outside the main peak, which reduces the effective size of the array.

III. Error Correction Method

In order to mitigate the performance degradation and to exploit the full resolution of the array, it is necessary to correct the error caused by the range-angle coupling. The additional path difference ΔR_k of the received signal at the k-th virtual channel can be described by a frequency shift of the beat signal measured at the array center. To obtain overlaying range spectra for all channels [Fig. 2 (a)], a frequency shift of the measured signal $s_{\text{B},k}$ is performed by

$$s_{\text{B,corr},k}(t) = s_{\text{B},k}(t) \exp\left(-\text{j}2\pi \frac{2\Delta R_k}{c_0} \frac{B}{t_{\text{up}}} t\right), \qquad (2)$$

where $s_{\text{B,corr},k}$ is the corrected signal, $t \in [0, t_{\text{up}}]$ is the continuous time, t_{up} the up-chirp time, B the modulation bandwidth, and c_0 the speed of light. As shown in (1), the frequency shift depends on the unknown incidence angle ϑ and the VX antenna position $x_{\text{VX}_{k,\phi}}$. The latter one is known from the manufacturing data or can be determined from the calibration data [7]. To obtain an a-priori knowledge of the incidence angle ϑ, the DoA estimation is split in two steps:

1) Perform an initial DoA estimation without any correction. This provides a DoA estimation with reduced angular resolution as not all channels are perfectly used.
2) Use the angular information from 1) as a-priori knowledge to perform a frequency correction. Afterwards, the DoA estimation is repeated and the full resolution capability of the array is exploited.

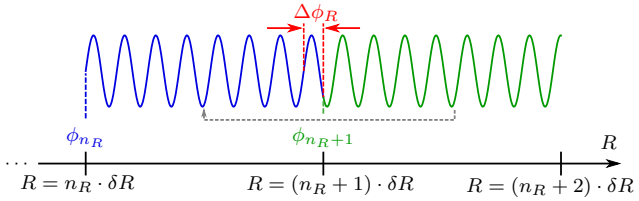

Fig. 3. Sketch of the resulting phase step for a shift of the range bin.

Due to the digitization of the measurement data and a subsequent FFT evaluation, a computationally efficient way to correct the error caused by the range-angle coupling is to shift the range spectra by multiples of the size of a range bin. The required number of range bins in order to shift the range spectra is calculated for the k-th virtual channel by

$$n_{\text{shift,k}} = \left\lfloor \frac{x_{\text{VX}_{k,\phi}}}{2} \sin(\vartheta) \frac{N_{\text{ZP}}}{\delta R} + 0.5 \right\rfloor, \qquad (3)$$

where N_{ZP} is the zeropadding factor and $\lfloor \cdot \rfloor$ denotes the floor function. In Fig. 3, the continuous phase of the beat signal is depicted over two range bins. A range shift according to (3) leads to a phase step if the size of the range bin is not an integer multiple of the wavelength. Thus, an additional phase correction has to be applied to correct the frequency shift as in (2). This procedure avoids a repeated 2D-FFT processing for each target and angle. The necessary phase shift $\Delta\phi_{R,k}$ for the k-th virtual channel is determined by the ratio of the size of a range bin δR and the free-space wavelength λ_0, which is afterwards converted to a phase value according to

$$\Delta\phi_R = -n_{\text{shift,k}} \left(\frac{\delta R}{\lambda_0} - \left\lfloor \frac{\delta R}{\lambda_0} \right\rfloor \right) \cdot 360°. \qquad (4)$$

IV. Verification by Measurements

The range-angle coupling effect described in Section II is now verified by measurements. Afterwards, the effectiveness of the used correction method is demonstrated by measuring an extended target causing multiple target reflections.

A. Radar Demonstrator

The photograph and virtual array configuration of the time-division-multiplex MIMO radar consisting of 16 radar MMICs are shown in Fig. 4. It operates at the frequency at 160 GHz with a center frequency $f_c = 152.5$ GHz and bandwidth $B = 10$ GHz Each MMIC incorporates one TX and RX antenna. The radar parameters are summarized in Table 1.

B. Angular Estimation Performance

In the following, the theoretical lower resolution limits of the considered radar demonstrator are determined. The range resolution δR of the radar is given by [9]

$$\delta R = \frac{c_0}{2B} = \frac{c_0}{2 \cdot 10\,\text{GHz}} \approx 1.5\,\text{cm}. \qquad (5)$$

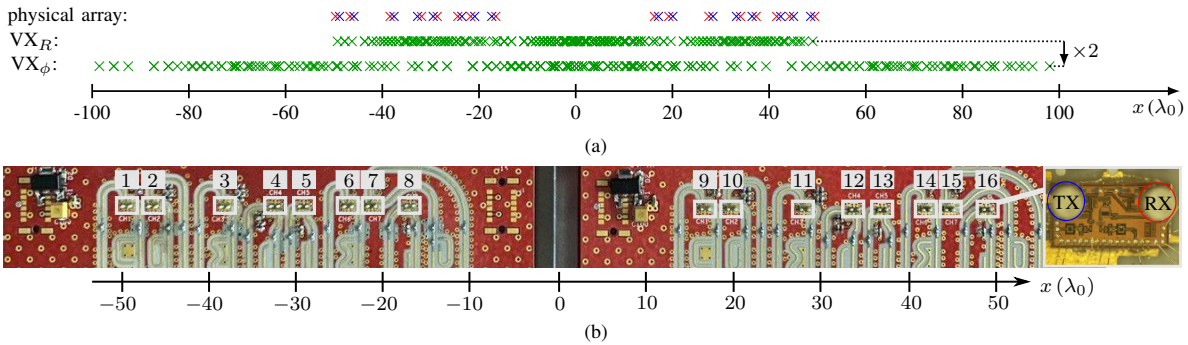

Fig. 4. (a) Sketch of the used antenna array with TX antennas (×), RX antennas (×), and VX antennas (×). (b) Photograph of the antenna array.

Table 1. Overview of the Radar Parameters

Ramp duration T	100 µs
Ramp repetition time T_r	150 µs
Center frequency f_c	152.5 GHz
RF bandwidth B	10 GHz
Number of chirps N_c	512
Number of virtual channels N_VX	$256 = 16 \times 16$
Virtual aperture A_V	$196.5\,\lambda_0$

The angular resolution $\Delta\vartheta$ of a radar (narrowband assumption) can be approximated by the 3 dB-beamwidth of the array or alternatively by the Rayleigh criterion, which is given by [10]

$$\Delta\vartheta = \frac{360^\circ}{2\pi} \cdot 1.22 \frac{\lambda_0}{A_\mathrm{V}} \approx 0.36^\circ \tag{6}$$

with the virtual aperture size A_V of the array.

In order to evaluate the radar performance, measurements are performed for a single target, which is located at the distance $R = 1.55\,\mathrm{m}$ and the angle $\vartheta = 35^\circ$. To show the performance improvement in the DoA estimation, the measurement results are compared to the conventional radar signal processing without a frequency and phase correction. In Fig. 5 (a), the range spectra for all 256 virtual channels are shown. It is apparent that without the correction of the error caused by the range-angle coupling, the radar responses of the single target are distributed over 8 range bins [cf. (3)]. After non-coherent integration, the target peak is significantly broadened [see Fig. 5 (b)]. The phase values of each virtual channel used for DoA estimation are extracted from one single range bin where the target is detected in the accumulated range-Doppler matrix. Without the correction of the error caused by the range-angle coupling, the phases of the targets in the radar response for most of the virtual channels are extracted outside the main peak or from noise [cf. Fig. 2 (b)]. This leads to a significantly reduced angular resolution as shown in Fig. 5 (c). Applying the corrections according to Section III, the radar responses from all channels are shifted to a single range bin. This leads to a sharp target peak and a correct phase extraction [see Fig. 5 (b)]. Consequently, an angular resolution close to the theoretical limit is achieved [see Fig. 5 (c)]. The sidelobe level of $-8\,\mathrm{dB}$ is caused by the array configuration.

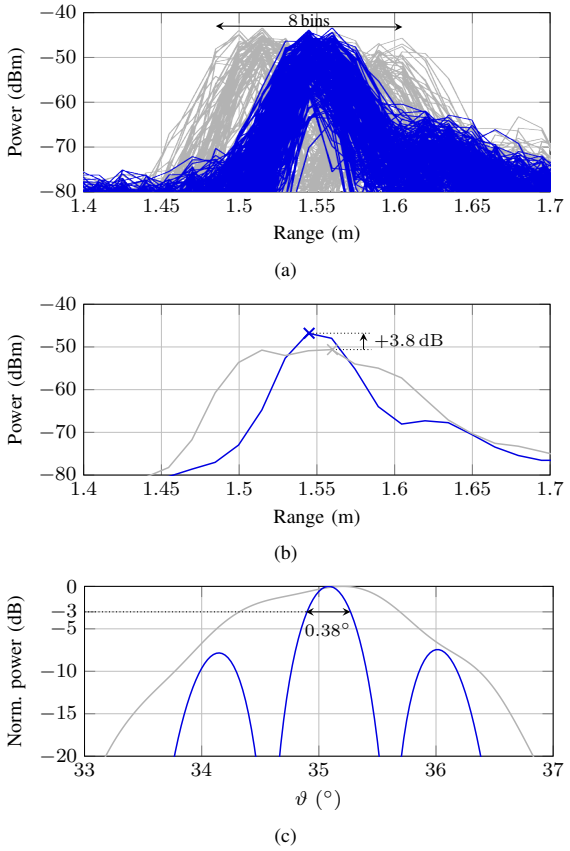

Fig. 5. Measured system performance of a target at $\vartheta = 35^\circ$ with correction of the error caused by the range-angle coupling (——) and without correction (——): (a) Range spectra for all virtual channels, (b) accumulated range spectrum, and (c) angular spectrum.

C. Extended Target

To demonstrate the effectiveness of the proposed signal processing method, a wooden box as shown in Fig. 6 (a) is used as an extended target. The box is rotating with a rotational velocity $v_\mathrm{r} = 35^\circ/\mathrm{s}$ around its vertical axis. To verify the range-angle coupling effect, the target is positioned at off-boresight angle of the array. The radar is calibrated

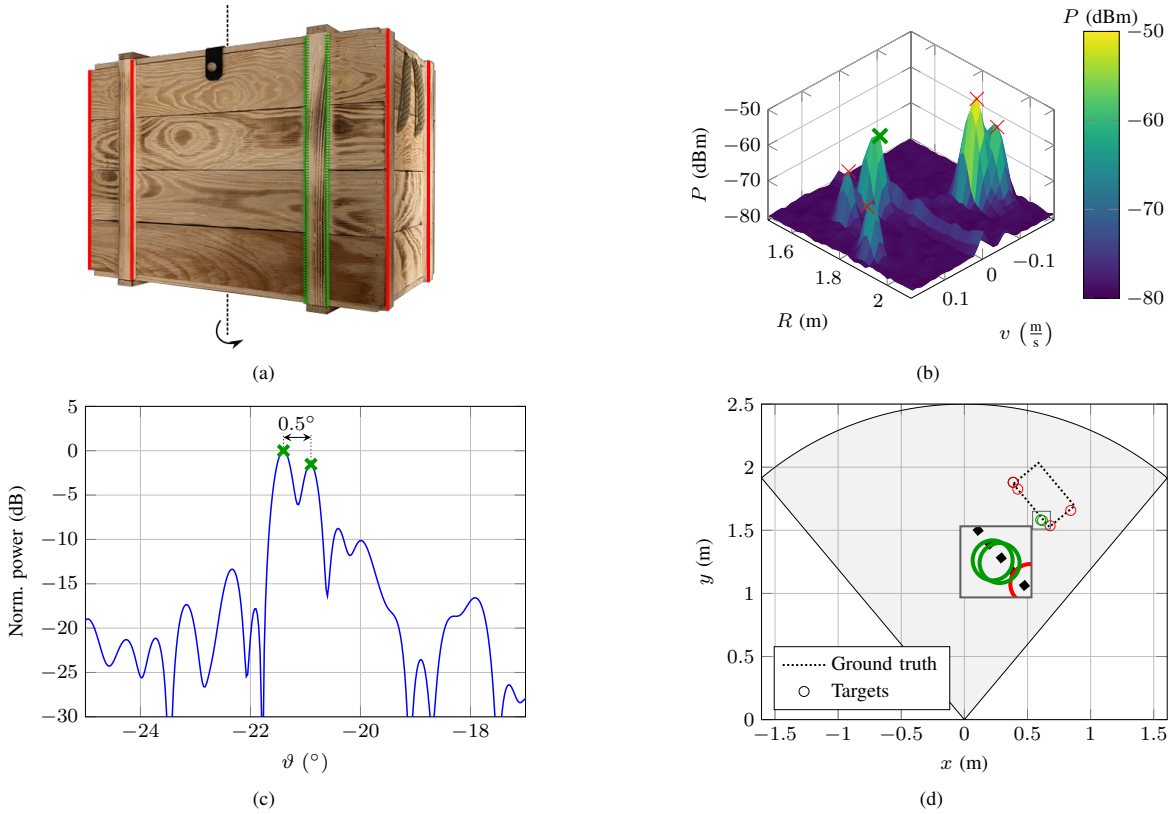

Fig. 6. Measurement of a wooden box located at off-boresight direction. (a) Photograph of the box. (b) Range-velocity diagram for a correction of $\vartheta \approx -21°$. (c) Angular spectrum for the detected wooden slat (✕) after correction of the range-angle coupling. (d) x–y diagram of the measurement scenario.

at the distance $R = 1.5\,\mathrm{m}$. Applying the correction method from Section III, an increase of the received power level for the corrected target is visible in the range-velocity diagram [Fig. 6 (b)]. Additionally, it is possible to detect the edges of a vertical wooden slat mounted at the wooden box, which have a difference in angle of only $0.5°$ [Fig. 6 (c)]. As shown in the x–y diagram it is possible to determine all significant edges and to determine the orientation of the wooden box.

V. Conclusion

In this paper, the performance degradation in radar imaging using electrically large arrays and high range resolution with conventional signal processing is discussed. In the given case, the difference in path length of the incident wave at the antenna elements exceeds the range resolution of the radar. Therefore, the measured distance of the target at the different receiving channels is distributed over several range bins depending on the unknown DoA. A signal processing method is proposed to correct the distribution of the range spectra and to exploit the full resolution capabilities of the array. Measurements of an extended target show the increase in resolution and prove the effectiveness of the proposed signal processing method.

Acknowledgment

This work was funded by the German Research Foundation with the project number 317632307.

References

[1] T. Spreng *et al.*, "Wideband 120 GHz to 140 GHz MIMO Radar: System Design and Imaging Results," in *European Microwave Conference*, Sep. 2015, pp. 430–433.

[2] S. Kueppers *et al.*, "A Compact 120 GHz SiGe:C based 2×8 FMCW MIMO Radar Sensor for Robot Navigation in Low Visibility Environments," in *European Radar Conference*, Oct. 2017, pp. 122–125.

[3] A. Dürr *et al.*, "High-Resolution 160-GHz Imaging MIMO Radar Using MMICs With On-Chip Frequency Synthesizers," *IEEE Trans. Microw. Theory Techn.*, pp. 3897–3907, Sep. 2019.

[4] R. Feger *et al.*, "A 77-GHz FMCW MIMO Radar Based on an SiGe Single-Chip Transceiver," *IEEE Trans. Microw. Theory Techn.*, vol. 57, no. 5, pp. 1020–1035, May 2009.

[5] S. Lutz *et al.*, "Lens based 77 GHz TDM MIMO Radar Sensor for Angular Estimation in Multitarget Environments," in *European Radar Conference*, Oct. 2013, pp. 212–215.

[6] P. Hügler *et al.*, "Radar Taking Off: New Capabilities for UAVs," *IEEE Microwave Magazine*, vol. 19, no. 7, pp. 43–53, Nov. 2018.

[7] A. Dürr *et al.*, "On the Calibration of mm-Wave MIMO Radars Using Sparse Antenna Arrays for DoA Estimation," in *European Radar Conference*, Oct. 2019.

[8] D. Bleh *et al.*, "W-Band Time-Domain Multiplexing FMCW MIMO Radar for Far-Field 3-D Imaging," *IEEE Trans. Microw. Theory Techn.*, vol. 65, no. 9, pp. 3474–3484, Sep. 2017.

[9] J. Li *et al.*, *MIMO Radar Signal Processing*. Wiley-IEEE Press, 2008.

[10] E. Hecht, *Optics*. Pearson Education Limited, 2017.